Short Article

Cell Stem Cell

Vascularized and Complex Organ Buds from Diverse Tissues via Mesenchymal Cell-Driven Condensation

Graphical Abstract

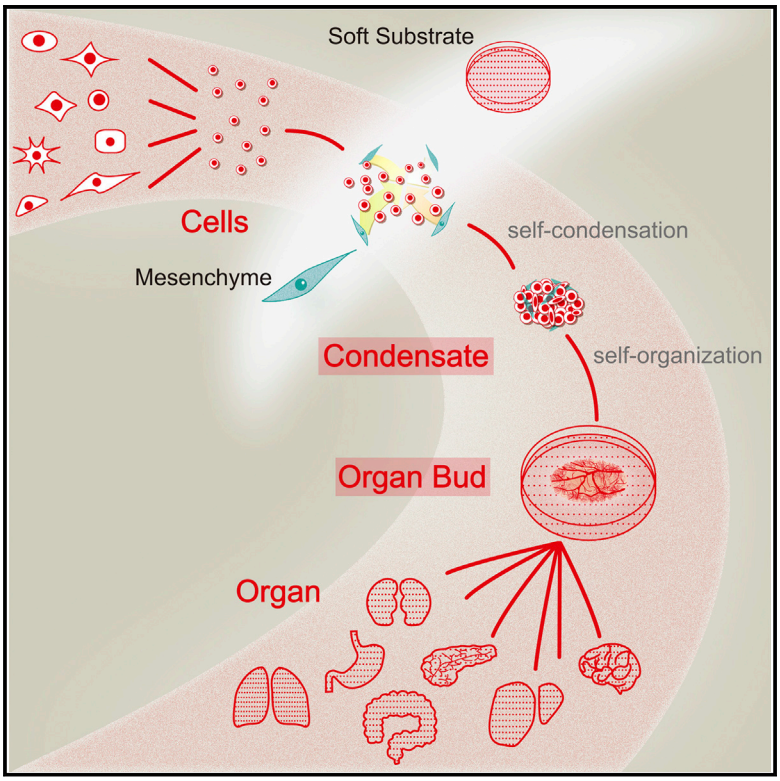

Authors

Takanori Takebe,
Masahiro Enomura, ...,
Hiroshi Y. Yoshikawa, Hideki Taniguchi

Correspondence

ttakebe@yokohama-cu.ac.jp (T.T.),
hiroshi@mail.saitama-u.ac.jp (H.Y.Y.)

In Brief

Takebe et al. report a generalized method for organ bud formation from diverse tissues, including kidney, pancreas, intestine, heart, lung, and brain, using heterotypic cell mixtures including mesenchymal stem cells to guide cell condensation. After transplantation, renal and pancreatic buds are readily vascularized and exhibit tissue-specific organization and function.

Highlights

- Transplantable organ buds self-assemble from diverse and heterotypic cells
- Mesenchyme-driven condensation on soft matrix is crucial for organ bud generation
- Transplanted diverse organ buds quickly become vascularized in vivo
- Vascularized organ buds generate functional tissues via in vivo self-organization

Accession Numbers

GSE66454

Takebe et al., 2015, Cell Stem Cell *16*, 556–565
May 7, 2015
http://dx.doi.org/10.1016/j.stem.2015.03.004

CellPress

CellPress

Cell Stem Cell
Short Article

Vascularized and Complex Organ Buds from Diverse Tissues via Mesenchymal Cell-Driven Condensation

Takanori Takebe,[1,2,5,6,*] Masahiro Enomura,[1] Emi Yoshizawa,[1] Masaki Kimura,[1] Hiroyuki Koike,[1] Yasuharu Ueno,[1] Takahisa Matsuzaki,[3] Takashi Yamazaki,[3] Takafumi Toyohara,[4] Kenji Osafune,[4] Hiromitsu Nakauchi,[5] Hiroshi Y. Yoshikawa,[3,*] and Hideki Taniguchi[1,6]

[1]Department of Regenerative Medicine, Yokohama City University Graduate School of Medicine, Kanazawa-ku 3-9, Yokohama, Kanagawa 236-0004, Japan
[2]PRESTO, Japan Science and Technology Agency, 4-1-8, Honcho, Kawaguchi, Saitama 332-0012, Japan
[3]Department of Chemistry, Faculty of Science, Saitama University, Shimo-okubo 255, Sakura-ku, Saitama 338-8570, Japan
[4]Center for iPS Cell Research and Application, Kyoto University, 53 Kawahara-cho, Shogoin, Sakyo-ku, Kyoto 606-8507, Japan
[5]Institute for Stem Cell Biology and Regenerative Medicine, Stanford University School of Medicine, Stanford, CA 94305, USA
[6]Advanced Medical Research Center, Yokohama City University, Yokohama, Kanagawa 236-0004, Japan
*Correspondence: ttakebe@yokohama-cu.ac.jp (T.T.), hiroshi@mail.saitama-u.ac.jp (H.Y.Y.)
http://dx.doi.org/10.1016/j.stem.2015.03.004

SUMMARY

Transplantation of in-vitro-generated organ buds is a promising approach toward regenerating functional and vascularized organs. Though it has been recently shown in the context of liver models, demonstrating the applicability of this approach to other systems by delineating the molecular mechanisms guiding organ bud formation is critical. Here, we demonstrate a generalized method for organ bud formation from diverse tissues by combining pluripotent stem cell-derived tissue-specific progenitors or relevant tissue samples with endothelial cells and mesenchymal stem cells (MSCs). The MSCs initiated condensation within these heterotypic cell mixtures, which was dependent upon substrate matrix stiffness. Defining optimal mechanical properties promoted formation of 3D, transplantable organ buds from tissues including kidney, pancreas, intestine, heart, lung, and brain. Transplanted pancreatic and renal buds were rapidly vascularized and self-organized into functional, tissue-specific structures. These findings provide a general platform for harnessing mechanical properties to generate vascularized, complex organ buds with broad applications for regenerative medicine.

INTRODUCTION

Current stem cell therapies primarily target diseases that are treatable by cell transplantation, which is accomplished via cell-type specification of stem cells and reprogramming factors (Sasai, 2013b). However, these prevailing transplantation approaches produce limited clinical therapeutic outcomes as well as potential side effects compared with organ-based therapy (also termed organ transplantation). Given the limitations of cell-based approaches, the development of innovative technologies that enable the reconstitution of 3D organs from stem cells is urgently required to potentially address the severe donor organ shortage and to lower the high medical costs incurred by the increasing numbers of waiting patients.

Despite the recent remarkable progress in "organoid technology," including the generation of the optic cup (Eiraku et al., 2011), the pituitary epithelium (Suga et al., 2011), the intestine (Sato and Clevers, 2013), and the cerebrum (Lancaster and Knoblich, 2014), the reported examples are composed entirely of epithelial structures and generally lack complex structures such as blood vessels. These characteristics limit their application, especially in the context of clinical transplantation. Specifically, much of the reported examples have relied on tissues with a high level of intrinsic self-organizing capacity from unilineage progenitor aggregates such as pluripotent stem cells; however, the likelihood of growing a complex and well-vascularized organ in dishes has seemed much less plausible (Ding and Cowan, 2013).

In general, the organ develops from a condensed tissue mass prior to blood perfusion, termed the "organ bud," emerging at early stages of organogenesis through the process of cell condensation. For instance, the multicellular orchestration that occurs between mesenchymal cells, undifferentiated vascular endothelial cells, and endoderm cells is required for the initiation of 3D liver bud condensation, which is characterized by a drastic delamination from an endodermal sheet-like tissue (Matsumoto et al., 2001). By mimicking this early organogenetic event, we have recently developed a groundbreaking culture method for deriving a 3D and transplantable organ bud in a dish from human induced pluripotent stem cells (iPSCs) cocultured with mesenchymal and endothelial progenitors. This system enables multiple progenitors to interact in a 4D (spatiotemporal) manner in vitro and in vivo, demonstrating the growth of a vascularized and functional organ via a human iPSC-derived organ bud transplant (Takebe et al., 2012, 2013, 2014b). The most notable aspect of our previous findings is the extremely large-scale morphogenetic changes that occurred even in 2D culture, in which transplantable tissues can be grown on a millimeter or even a centimeter scale from multiple heterotypic cell collectives.

The next critical steps would be to gain insight regarding the mechanisms underlying this dynamic process in culture and to

evaluate the translatability of such regenerative methods in other organ systems. The primary purpose of the present study was to dissect the mechanism of 4D self-assembly at the cellular level using integrated computational and biological approaches combined with live imaging analysis and to define the essential parameters required for the reproduction of this culture, including the environmental culture conditions. Next, we evaluated the adaptability of our proof-of-principle approach in multiple organ systems of health and disease, and finally, we determined the self-organizing capacity of vascularized and functional tissues by organ bud transplantation.

RESULTS

Quantitative Imaging Analysis Suggests the Presence of Contractile Mechanisms for Self-Driven Behaviors in Culture

To elucidate the mechanisms underlying the observed surprising degree of collective behavior, we initially tracked cellular movements during organ bud formation by performing a time-lapse imaging analysis. Human iPSC-derived hepatic endoderm cells, umbilical cord-derived endothelial cells (HUVECs), and mesenchymal stem cells (MSCs) were labeled with distinctive fluorescent markers and cocultured on a solidified matrix gel as previously described (Takebe et al., 2013). Live cell tracking revealed that after rapid cell convergence, the assembly of vascularized organ buds was initiated (Figures 1A and 1B); this was followed by subsequent spatial rearrangements via self-organization, as demonstrated by the formation of an endothelial-like network (Figure 1B, lower right). During the initial self-convergent phase, we discovered the formation of a cohesive multicellular unit that behaved as a group and consisted of cells that quickly traveled to a single center, a process termed collective condensation (Figure 1A).

To further understand the early dynamics of 3D organ bud formation, a time course of the condensate shape was evaluated using live imaging (Figures 1B and 1C). Estimation of the averaged radius of the condensate, which was calculated as $\sqrt{(A/\pi)}$ (where A is the projected area of the condensate), clearly revealed that the edge of the condensate moved toward its center at a rate of <10 μm/h in $t \leq 7$ hr and then accelerated to 400 ~500 μm/h over the next several hours (Figure 1C), exhibiting parallel dynamics throughout both x and y axes (Figure 1B). Subsequently, the radius of the organ bud converged exponentially to ~2 mm. By contrast, its circularity, a structural parameter that indicates how closely the shape of an object approaches that of a circle, decreased monotonically from the beginning of the cell culture and reached a minimum value of ~0.5 at t = ~10 hr. The circularity then increased and finally achieved a constant value of ~0.85 at t = ~20 hr (Figure 1C).

The maximum velocity of the condensate edge, 400 ~500 μm/h, was much higher than that reported for cell migration (Dourdin et al., 2001; Wolf et al., 2003), which indicated that the formation of the condensate was based not on active cell migration but on cell contraction. In addition, the serial measurements of the condensate size from t = ~15 hr (red line in Figure 1C) suggested that the collective behaviors could be approximated with a predictive curve (dotted line in Figure 1C) generated using the Kelvin-Voigt model, implying that the formation of tissue-level cumulative stress fibers might at least trigger this process (Figure 1C). Indeed, the Kelvin-Voigt model, which is a simple viscoelastic model that contains a dashpot with viscosity and a spring of stiffness k connected in parallel, is described by an exponential function, $A\exp(-t/\tau) + B$, and has commonly been used to study the viscoelastic behaviors of various tissues and cytoskeletal components such as stress fibers (Besser and Schwarz, 2007; Forgacs et al., 1998; Fung, 1993). Furthermore, the circularity results clearly showed that the shape of the condensates at $t \leq 10$ hr deviated from a circle (in 3D, a sphere). This observation correlates with the equilibrium state at which condensates of adhesive cells minimize the surface free energy of the system (Steinberg, 1962). These results indicate that the cumulative driving force for condensate formation at $t \leq 10$ hr increased due to the formation of stress fibers and cell-cell junctions; however, the driving force still did not exceed the adhesion strength of the cell-extracellular environment.

MSC-Dependent Cytoskeletal Contraction Is Essential for Cell-Collective Behaviors

To identify the critical cell types for this dynamic and directed collective movement, we examined all of the possible combinations of the three cell lineages. Clearly, the lack of MSCs in the coculture led to a failure in condensate formation, but a single MSC culture was not sufficient for termination, revealing that the presence of MSCs triggered the initiation of self-condensation (Figure 1D). Although we exposed HUVECs and iPSC-HEs (iPSC-derived hepatic endoderm cells) to the condition medium generated by MSCs, no condensing phenomena were observed (data not shown). To test the ''contraction mechanism'' implied by the above-mentioned observation, we evaluated the contributions of the contraction force of the MSCs at the molecular level against both their substratum and the surrounding cells. During embryonic invagination, a group of cells undergoes constriction. The drastic inward displacement of cell-cell junctions is driven by myosin II (MII) activity, allowing cells to invaginate during embryonic gastrulation (Bertet et al., 2004; Pouille et al., 2009; Shindo and Wallingford, 2014). Di-phosphorylation of the MII regulatory light chain (ppMRLC) possesses a greater actin-activated Mg^{2+}-ATPase activity than monophosphorylated MRLC (pMRLC) to produce a contractile force (Mizutani et al., 2006). This knowledge led us to evaluate MII activity by measuring the time-course-dependent changes in the amount of MRLC, pMRLC, and ppMRLC by western blot analysis. We showed a significant peak in ppMRLC after 4 hr of plating as well as an increase in the total amount of MRLC during the condensate-forming process, which corresponded to the time at which cells initiate their collective movements (Figure 1E). As a consequence, ppMRLC is known to significantly enhance MII ATPase activity for producing contractile force (Straight et al., 2003). Consistently, we found that this condensate formation could be completely antagonized by treatment with blebbistatin (an MII ATPase inhibitor) (Figure 1F). In parallel, similar to published results (Shin et al., 2014; Shutova et al., 2012), blebbistatin significantly increased MIIA phosphorylation at S1943 (pS1943: inactivates MIIA activity) at 6 hr, as measured by intracellular flow cytometry and western blot analysis, respectively (Figures 1G and 1H). Similarly, the addition of a Rho kinase inhibitor, Y-27632, to the cocultures partially delayed condensate

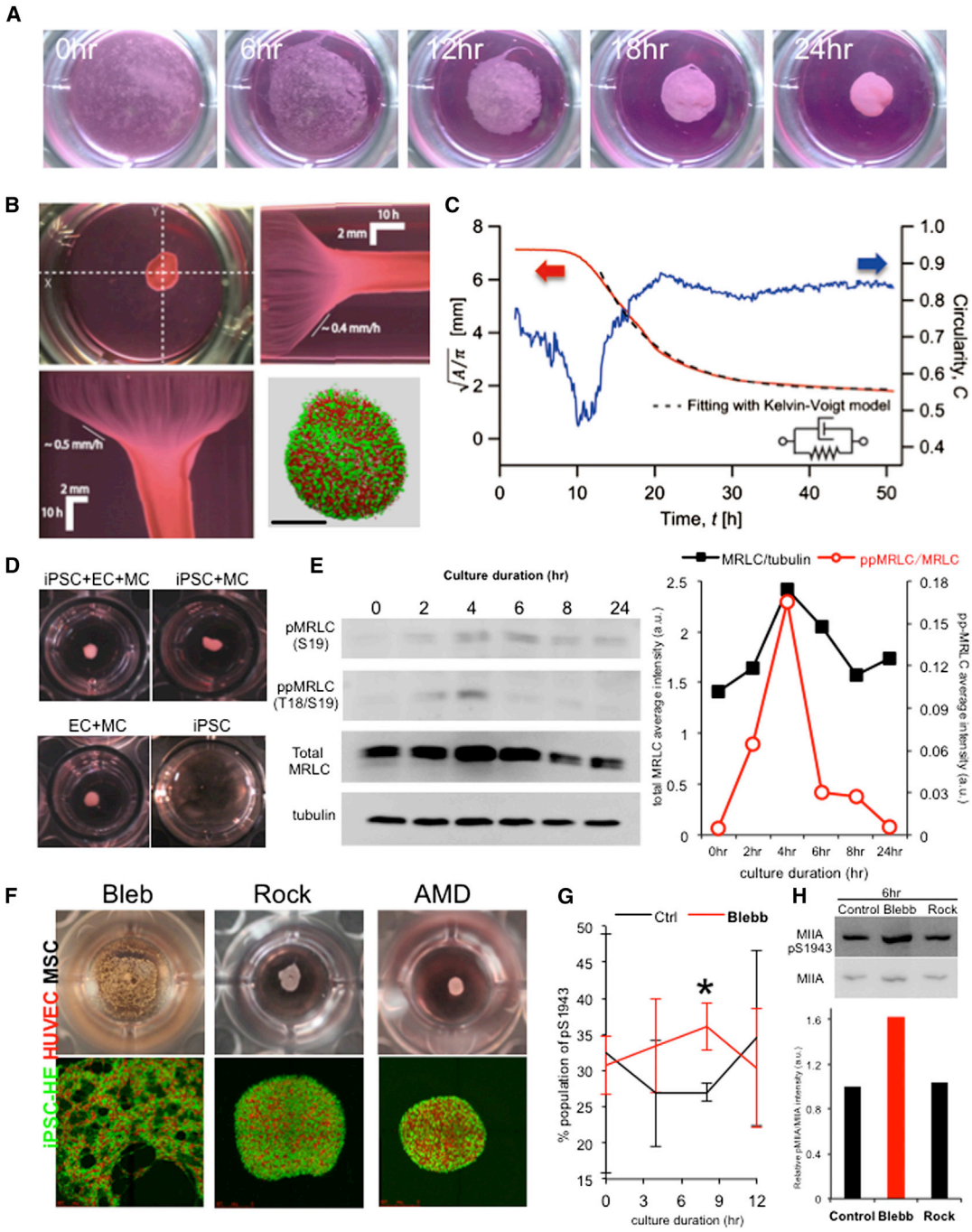

Figure 1. Mesenchymal Cell-Driven Contraction Is Essential for the Dynamic Condensation of Heterotypic Cell Collectives

(A) Self-driven rapid condensation of human iPSC-derived hepatic cells.

(B) Parallel dynamics of the movement of the condensate edge on both the x and y axes during condensation. Green, human iPSC-hepatic cells; red, HUVECs; unlabeled, MSCs. Bar, 740 μm.

(C) Structural analysis of 3D organ bud formation dynamics. The source movie is Movie S1 from our previous paper (Takebe et al., 2013). *A* is the projected area of the organ bud (red). Circularity was defined as $4\pi A$ divided by the square of the contour line length, L^2(blue). The black dotted line is a curve that fits with the Kelvin-Voigt model.

(D) Examination of all possible combinations of three lineages. iPSC, iPSC-derived hepatic endoderm cells; EC, HUVECs; MC, hMSCs.

(E) Western blot analysis using total MRLC, pMRLC, and ppMRLC antibodies with total cell lysates at specific time points.

(F) Pharmacological inhibition of dynamic condensation.

(G) Blebbistatin treatment significantly increased the inactive form of MIIA after 8 hr of culture (data represent the means ± SD, n = 3, *p < 0.05). AMD, AMD3100; Rock, Rho kinase inhibitor Y-27632; Bleb, blebbistatin.

(H) Western blot analysis using antibody against pS1943 with untreated and drug-treated cells at 6 hr.

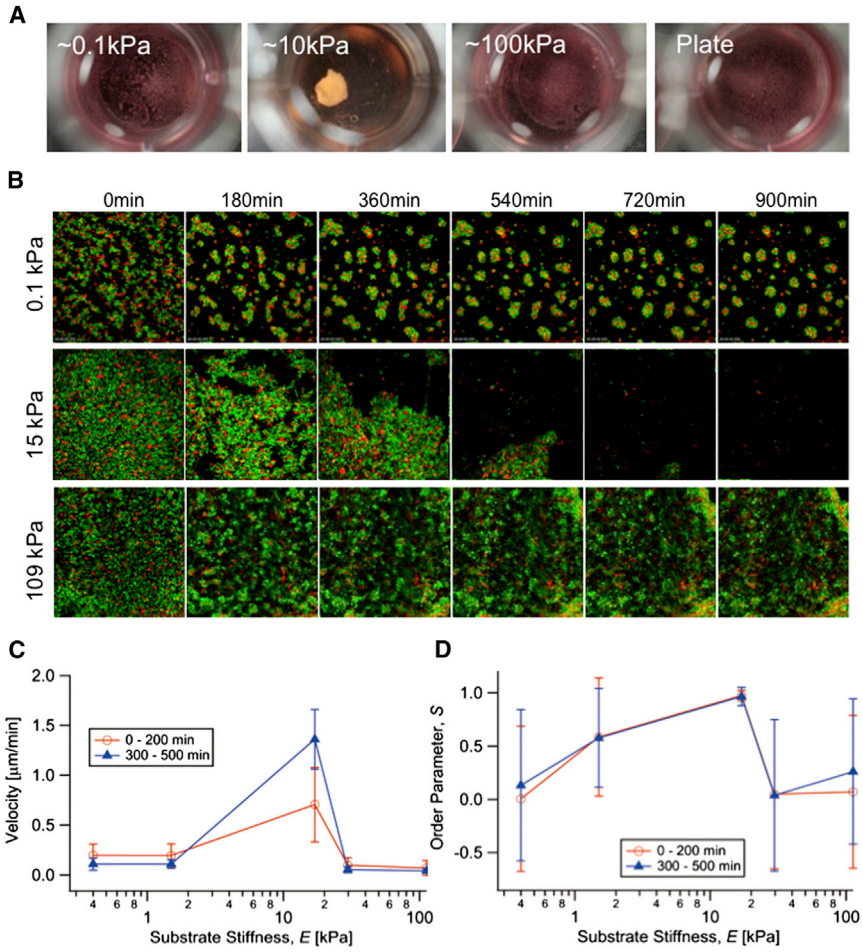

Figure 2. Stiffness-Directed Contraction Is Essential for Dynamic Condensation

(A) Stiffness optimization for dynamic condensation. An organ bud formed in culture is shown 2 days after plating.

(B) Time-lapse confocal microscopy of the condensate formation process. Each image was obtained by maximum intensity projections of a series of z stacks at the indicated time points. GFP-HUVECs and KO-hMSCs are shown.

(C and D) The velocity and order parameter (*S*) of the cell movement depend on the substrate stiffness. The red and blue lines represent the mean values for 0–200 min and 300–500 min, respectively. Error bars denote the standard deviation (SD). Note that the perfectly synchronized movement of cells yields $S = 1 \pm 0$, whereas *S* gets closer to 0 with a large SD during random movement.

formation, presumably through the phosphorylation of MRLC (Figures 1E, 1F and S1). In contrast, pharmacological inhibition of chemokine receptor pathways in response to the addition of AMD3100 did not hinder organ bud formation, although a recent report suggested the potential importance of a self-generated chemokine gradient during organogenesis (Figure 1F) (Donà et al., 2013). Furthermore, we have performed the immunostaining of MIIA in the sectioned organ bud, revealing that CD90+ MSCs significantly expressed MIIA at 24 hr of culturing (Figure S1B). These results clearly suggested that the MSC-based traction force produced by the actomyosin cytoskeletal axis plays an important role in the directed and drastic movements of cell collectives.

Self-Condensation Can Be Maximized by Soft Environmental Conditions in Culture

Cellular cytoskeletal contraction in culture is balanced by the degree of attachment to the anchoring matrix (Discher et al., 2005). Recent studies measuring the traction force of single cells have shown that cytoskeletal tension can be modulated by the biochemical and biophysical parameters of the substratum (Liu et al., 2010). Therefore, we assumed that the modulation of substratum conditions could alter the collective behavior of the cultured cells if the contraction mechanism is the correct explanation for this process. In our previous study, various biochemical conditions were tested utilizing hydrogels, collagens, laminin, entactin, and their combinations (Takebe et al., 2013). The results showed that a basement membrane composite, such as Matrigel, is the most efficient matrix. To further clarify the essential parameters, we assessed the effect of substrate stiffness using hydrogels with tunable elasticity. Here, MSCs and HUVECs were cocultured on Matrigel-coated hydrogels with different elastic moduli ($E \sim$0.1–100 kPa) and on a plastic plate ($E \sim$GPa). After incubation for 24 hr, significant differences in self-driven behavior were already discernible (Figure 2A): the cells on hydrogels with $E \sim$10–20 kPa organized into mm-sized large condensates, whereas the cells on softer or stiffer substrates formed smaller clusters ($\lesssim$100 μm). Fluorescence images also showed that the cells moved collectively and directionally only on substrates with a moderate stiffness (Figures 2B and S2). As shown in Figures 2C and 2D, both the velocity and order parameters exhibited maxima at E = 17 kPa. Such enhanced collective behaviors of cells on a gel substrate with intermediate stiffness indicate that the competition between cell-hydrogel and cell-cell interactions might be involved in the mechanism underlying the formation of cell condensates, especially in their initiation process. This observation clearly indicated that the formation of the condensate was driven by the interplay between cell-hydrogel and cell-cell interactions (Supplemental Discussion).

Translatability of the Contractile Principle to Other Organ Systems

Considering that the MSC-driven contraction force on defined stiffness is central to the observed self-driven behavior, we wondered whether this principle could be extended to organ systems beyond the barriers of the germ layer, with the goal of future applications in regenerative medicine. To address this practical question, we evaluated the adaptability of our proof-of-principle approach to other organs using multiple cells or

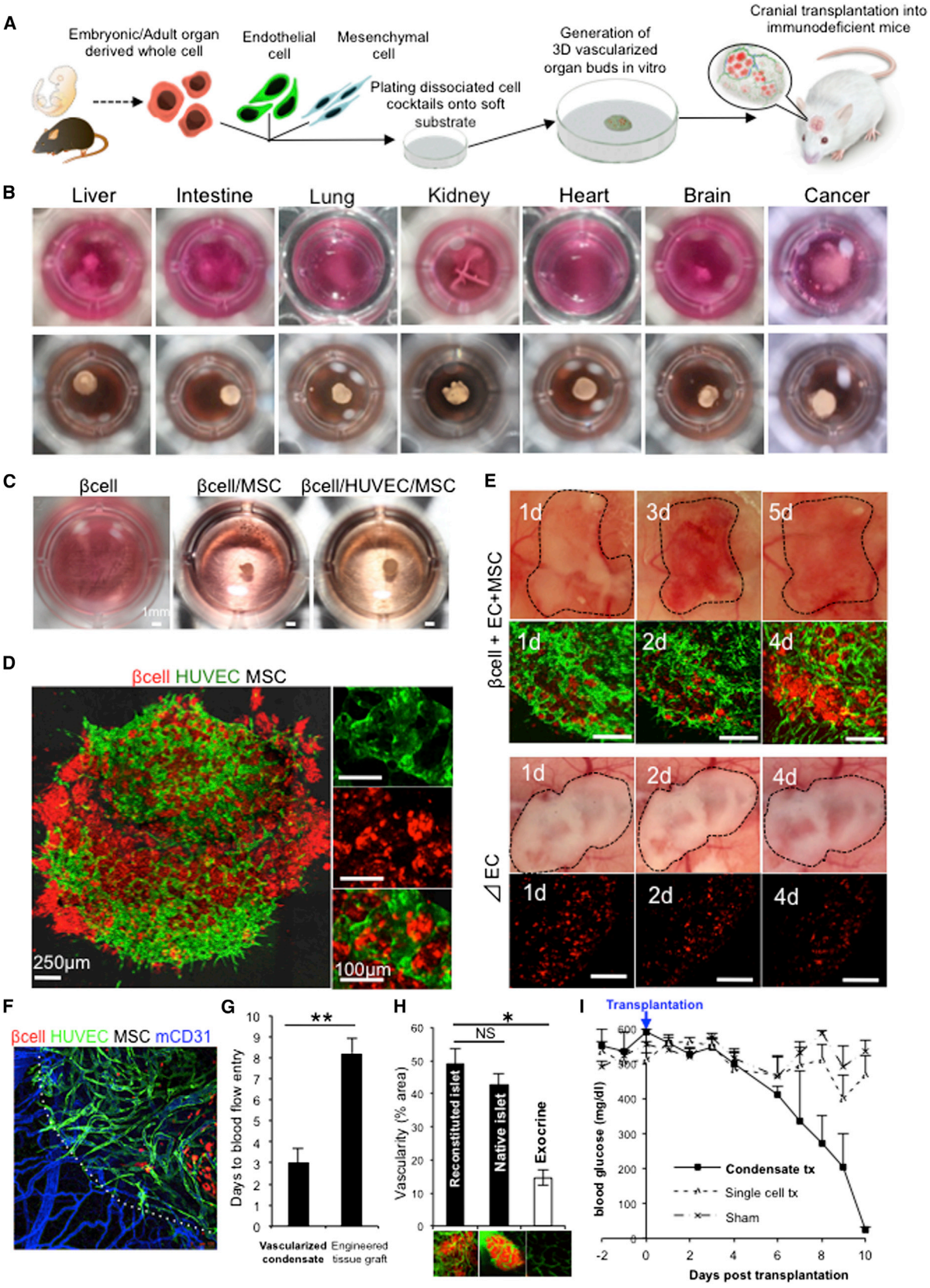

(legend on next page)

tissue fragments (up to 200 μm) isolated from adult mice (Figure 3A). Surprisingly, the dynamic condensation of cell collectives was maintained for all of the cell/tissue types tested, including liver, intestine, lung, heart, kidney, brain, and even cancer (HepG2) (Figure 3B). Time-lapse imaging analyses revealed that both the embryonic and adult cells autonomously formed a single 3D condensate that tolerated additional manipulations well, including transplantation (Figure S3A). When the condensates were designed to contain endothelial cells in culture, the transplanted tissues underwent a much more rapid perfusion with recipient circulation (average perfusion time: ~72 hr) (Figure S3B) compared with reliable conventional tissue engineering approaches (average perfusion time: ~192 hr) (Figure 3G). This result suggested that scaffold-free and self-condensation approaches are superior for the induction of vascularization. Although the presence of endothelial cells was dispensable for the generation of condensates, the post-transplant outcomes were clearly disappointing in the absence of HUVECs because no signs of functional vascularization were observed in vivo (Figure S3B, right).

Next, we selected pancreatic cells for in-depth characterization due to the increasing evidence that the pancreas follows a developmental program similar to that of the liver (Lammert et al., 2001). Dissociated murine β cells (MIN6) were cocultured with HUVECs and MSCs, resulting in dynamic condensate formation similar to that observed in the liver bud experiments (Figure 3C). After 4 days of culture with endothelial medium, the condensates developed into large, mechanically stable, 3D tissues that exhibited several signs of self-organization (Figure 3D). Furthermore, the transplantation of a 3D pancreatic condensate resulted in rapid reperfusion and stimulated successful β cell engraftment (Figure 3E). After 14 days, the transplants developed islet-like structures with functional microvascular networks (Figure S4A) that were connected to the recipient circulatory system (Figures 3F and 3G). Consistent with previous reports, the intravital quantification of the functional vascular density showed that the capillary network was 4.2-fold denser in the reconstituted islet-like tissues compared to the surrounding tissues (Figure 3H and Movie S3). The inner part of the islet-like tissues contained human endothelial cells with basement membrane, which is known to support β cell function (Figures S4B and S4C). To evaluate their therapeutic potency, in-vitro-derived condensates were transplanted into the kidney subcapsule of a type 1 fulminant diabetic mouse model. The mice were successfully treated with a condensate transplant, as demonstrated by the rapid normalization of body weight and blood glucose levels. In contrast, mice transplanted with a single dispersed β cell showed delayed effects, presumably due to the transplant's failure to undergo vascularization and subsequent engraftment (Figure 3I). Thus, we experimentally demonstrated that this principle is applicable to other organ systems using an optimal cell population and successfully reconstituted vascularized and functional 3D tissues in vivo.

Functional and Vascularized Kidney Formation via In-Vitro-Grown Organ Bud Transplantation

Interestingly, we noticed that in some organs, embryonic cell-derived condensates, i.e., organ buds grown in vitro, were ultimately able to efficiently self-organize into functional tissues, whereas adult organ cell-derived condensates reconstituted tissues with a minimal resemblance to the original tissue after transplantation (Figures 4, S4D, and S4E). For example, the transplantation of reconstituted organ buds from embryonic day (E) 13.5 kidney-derived dissociated cells resulted in the development of glomerular-like microtissues after 8 days of transplantation followed by quick revascularization (Figures 4A and 4B). To provide additional definitive proof of self-organization, we generated a kidney bud in culture from mixed embryonic kidney cells dissociated from three distinctly labeled cell populations from E13.5 mice (beta-actin-GFP, -RFP, and -CFP), transplanted the bud inside the cranium, and performed repeated live imaging. Intravital confocal imaging at 14 days revealed the successful formation of multi-color integrated glomerular-like tissues (Figures 4C and S4F), confirming that the dissociated embryonic cells self-organized into a glomerular architecture in vivo. The infusion of high-molecular-weight FITC dextran via the systemic circulation with fluorescein-conjugated mouse CD31 antibody revealed the presence of a number of newly generated glomerular-like structures containing an abundant microcirculation at day 28 (Figures 4D and 4E). Notably, without the organ bud formation culture, E13.5 kidney-derived single-cell transplantation barely reconstituted such structures (Figure 4E, lower). To characterize the degree of maturation, global gene expression profiling was performed by focusing the reported kidney signature genes, which are known to be downregulated throughout development (Schwab et al., 2003). Hierarchical clustering analysis of the explants at day 14 and 28 and kidneys of multiple developmental stages revealed the successful maturation of the transplants into tissues corresponding to

Figure 3. Universal Culture Platform for Growing Self-Condensed Tissues from Hetero-Mixtures of Cell Collectives

(A) Schematic representations of organ bud formation experiments using a variety of organ systems.

(B) The MSC-based condensation principle is adaptable to all tissue types examined in this study, including intestine, lung, kidney, heart, brain, and even cancer cells. The two rows show a macroscopic view of the tissues before or after condensation.

(C and D) Macroscopic or confocal image of the self-condensed β cells. Red, β cell; green, HUVECs; unlabeled, hMSCs. Bar, 1 mm, 250 μm, and 100 μm.

(E) β cell-derived condensates were quickly vascularized by the recipient circulation in the presence of HUVECs, whereas the endothelial cell-absent condensate failed.

(F) Intravital visualization of human-mouse chimeric vessels on day 9. Red, β cell; green, HUVECs; blue, mouse-specific CD31; unlabeled, hMSCs.

(G) A comparison of the numbers of days required for functional blood vessel establishment between our vascularized condensate- and tissue engineering-based approaches (data represent the means ± SD, n = 6, $^{**}p < 0.01$).

(H) The vascular density (%) inside/outside of the reconstituted, native islets and exocrine pancreas, respectively (data represent the means ± SD, n = 6, $^{*}p < 0.05$, NS: not significant).

(I) Changes in blood glucose after in-vitro-grown condensate transplantation compared with the single dispersed β cell or sham transplanted groups (data represent the means ± SD, n = 3).

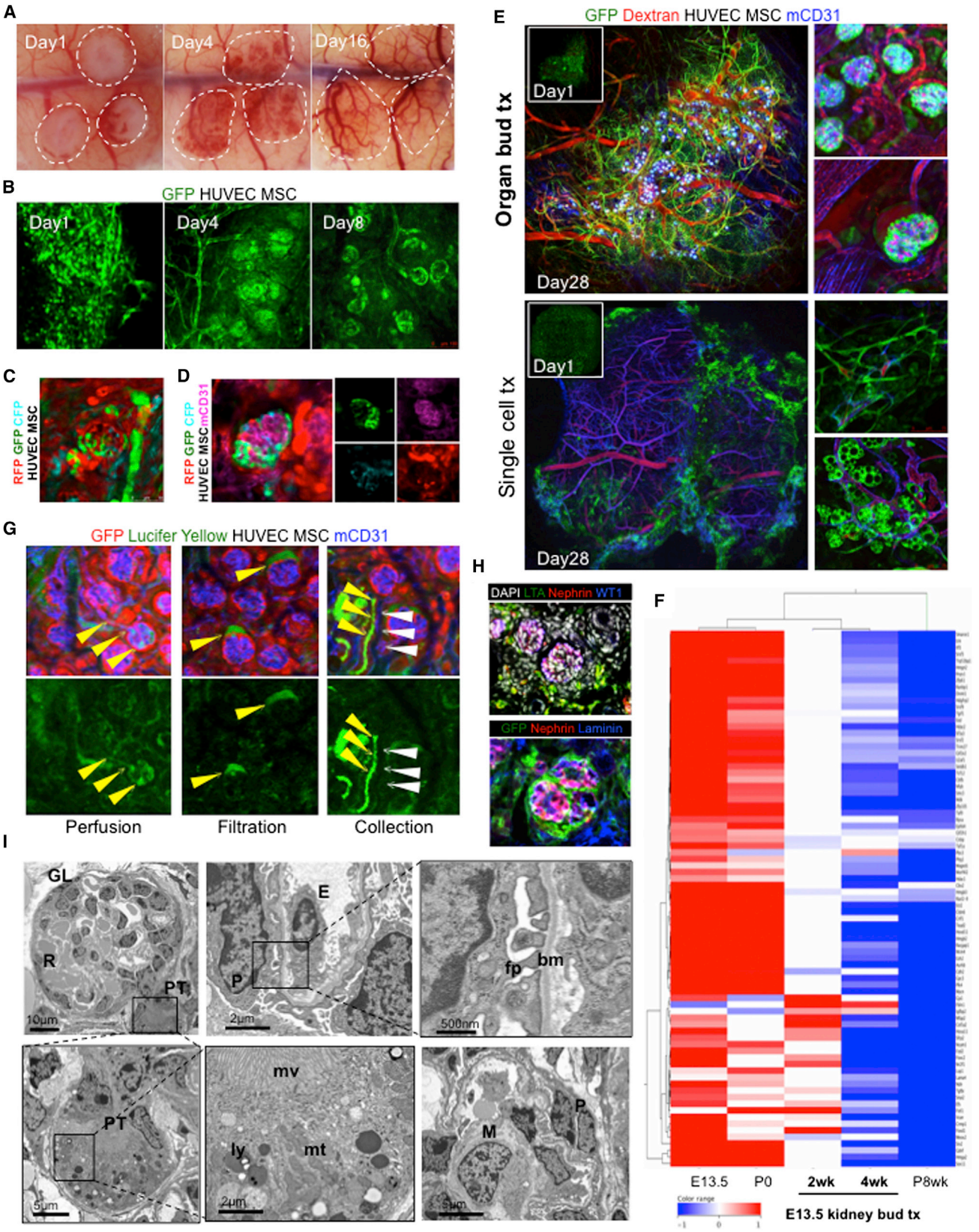

(legend on next page)

postnatal kidneys, compared to the original E13.5-derived primary tissue (Figure 4F).

Furthermore, to demonstrate the functionality, we injected Lucifer Yellow, a dye that is freely filtered in glomeruli, intravenously to label Bowman's space and subsequent excretion (Hackl et al., 2013). Repeated live imaging analysis identified multiple steps in urine production: initial perfusion into the glomerular capillaries (Figure 4G, left), primary filtration into the urinary space (Figure 4G, middle), and subsequent outflow into collecting systems (Figure 4G, right). The formation of slit proteins surrounding the basement membrane was confirmed by co-immunostaining of GFP, nephrin, and laminins in the explanted transplants at day 21 (Figure 4H, upper). Additional immunofluorescence confirmed the presence of WT1 (Wilms' tumor suppressor-1) and LTA (lectin Lotus tetragonobulus agglutinin) surrounding the developed glomeruli, suggesting the differentiation into podocytes and proximal tubule formation, respectively (Figure 4H, lower). Indeed, electron microscopy further confirmed the presence of podocytes with foot processes that were separated from the glomerular endothelium by a basement membrane (Figure 4I). Together, we concluded that immature organ buds grown from dissociated embryonic cells using our culture method would aid in generating the functional and vascularized kidney in vivo by maximizing the intrinsic self-organizing capacity of the cells.

DISCUSSION

In the 1960s, small aggregates of dissociated embryonic cells were shown to reconstitute tissues with an architecture resembling that of the original tissue via self-organization. After the required types and numbers of various cells had aggregated to allow the close interaction of the cells, individual cells were able to self-organize to form functional tissues in vitro (Takeichi, 2011). This classic knowledge is now being adapted into recent studies of brain, optic cup, and adenohypophysis derived from pluripotent stem cell-derived small cell aggregates (Sasai, 2013a). However, these previous self-organization studies, which used multi-well dishes with steep sides and rounded bottoms to the wells, generally started with micrometer-scale tiny aggregates, and such stem cell aggregates self-organized into entirely epithelial structures, limiting their utility to specific organs such as neural systems due to their marked propensity to self-organize in the absence of vasculatures. In addition to the limited scalability of the culture, none of the available culture systems have resulted in self-assembling tissue formation from optimal heterogeneous mixtures of cell collectives.

Considering both the dependence on the substrate stiffness and the requirement for MSCs, we concluded that MSC-driven contraction on a soft substrate condition should be one potential mechanism for the heterotypic collective behaviors. Previous study showed that visceral endoderm cells in non-muscle myosin heavy chain IIA knockout mouse do not differentiate, exhibiting the defects in cell adhesion and subsequent tissue organization prior to organ bud development in mouse embryonic cells (Conti et al., 2004). Combined with loss-of-function experiments such as knockdown-based approaches (Raab et al., 2012), future exploration of the contraction mechanism in organ bud self-organization in human iPSCs would elucidate a unique role of myosin for human organogenesis in a dish.

Thus, the present work demonstrates one promising principle: much larger-scale self-organized tissues can easily be assembled via condensation from desired multiple cell/tissue types. Self-assembled condensates, which are better defined than aggregates, could be used to examine the subsequent self-organizing potential of cells in vivo after transplantation. Endothelial cells were experimentally integrated into the condensates to assess the potential for rapid vascularization and subsequent functionalization. However, we and others are also interested in evaluating the substantial potential of other, unexplored supporting cell types, such as neural cells, to stimulate more precise tissue reconstitution.

Moreover, as evidenced by the kidney self-organization experiments presented herein, less mature tissues, or organ buds, generated through the condensation principle might be the most efficient approach toward the reconstitution of mature organ functions after transplantation, rather than condensates generated from cells of a more advanced stage. This concept is particularly important to note when adapting this to human pluripotent stem cell (Takebe et al., 2013) or adult stem cell (Takebe et al., 2014a) derivatives.

Further refinements are needed to determine the optimal conditions for targeted tissue self-organization; however,

Figure 4. Self-Organization of Functional and Vascularized Kidney via In-Vitro-Grown 3D Organ Bud Transplantation

(A) Macroscopic observation of transplanted in-vitro-grown kidney buds showing perfusion and sophistication of reconstituted blood vessels. The dotted area indicates the transplants.

(B) Intravital tracking of kidney buds showing in vivo dynamics of kidney development.

(C) Self-organization of glomerular structures from kidney bud generated from three distinct fluorescent embryonic mice after 14 days. Bar, 50 μm.

(D) mCD31-647 infusion study demonstrating the formation of multi-colored labeled, glomerular-like tissue with capillaries.

(E) Generation of functional nephrons from transplanted kidney buds at 28 days after transplantation under a cranial window. Tissues resembling glomeruli or tubular structures barely developed from the E13.5-dispersed cell transplant (right lower panel). Red, dextran; green, GFPs; blue, mouse-specific CD31; unlabeled, HUVECs and hMSCs.

(F) Comparison of kidney developmental gene signatures among in-vitro-derived kidney buds at 2 and 4 weeks after transplantation and primary kidneys (E13.5, 0 day [P0] and 8 weeks [P8wk] after birth).

(G) Intravital visualization of the renal functions of the generated glomeruli after 21 days of transplantation, including initial blood perfusion (left), primary filtration into Bowman's space (middle), and urinary outflow into collecting systems (right). Red, mouse GFP; green, Lucifer Yellow; blue, mouse-specific CD31; unlabeled, HUVECs and hMSCs. Yellow arrowhead, Lucifer Yellow; white arrowhead, Lucifer-Yellow-negative endothelial cells.

(H) Histological analysis of reconstituted tissues explanted at 21 days. Immunostaining for LTA, nephrin, WT1, GFP, and laminin is shown in each panel. Bars, 100 μm.

(I) Electron microscopy of kidney bud transplants at 21 days. GL; glomerulus; PT, proximal tubule; P, podocyte; E, capillary endothelium; R, red blood cell; M, mesangial cell; bm, basement membrane; fp, foot processes; mv, microvilli; ly, lysosome; mt, mitochondria.

proof-of-concept organ bud transplantation might be a rational approach toward the generation of vascularized and functional complex organs. This culture principle will not only be a powerful tool for the study of human developmental biology and pathology using pluripotent stem cells, but it will also facilitate the realization of next-generation generative medicine using in-vitro-grown complex tissue architectures for currently untreatable patients.

EXPERIMENTAL PROCEDURES

Self-Condensation Culture

To generate liver buds in vitro, we resuspended ~1–2 × 10^6 iPSC-hepatic cells, ~8–16 × 10^5 HUVECs, and ~2–4 × 10^5 hMSCs in a mixture of EGM and hepatocyte culture medium (HCM) (Cambrex) containing dexamethasone (0.1 μM, Sigma-Aldrich), oncostatin M (10 ng/ml, R&D Systems), HGF (20 ng/ml, Kringle Pharma, Inc.), and SingleQuots (Lonza) and plated them onto pre-solidified Matrigel (BD Biosciences) in a 24-well plate. Mechanically defined substrate (with methods described as follows) was mainly used in experiments shown in Figure 2. Regarding the mixture ratios for pancreatic or kidney tissue generation, we have adopted the following specific ratios. Pancreatic cells: HUVEC: MSC = 10:5:2, and kidney cells: HUVEC: MSC = 10:1:2, but this needs further intensive optimization. After ~4–6 days of culture, self-organized human iPSC-LBs (iPSC-derived liver buds) were analyzed using a Leica TCS SP8 confocal microscope (Leica Microsystems, Germany). To analyze the contribution of the substrate stiffness, we resuspended 2 × 10^6 HUVECs and 6 × 10^5 hMSCs in a mixture of EGM and seeded them on a substrate placed in a 24-well plate.

Statistical Analysis

The data for the biological assays are expressed as the means ± SD from three or five independent experiments. Comparisons between three or four groups were analyzed using Wilcoxon statistical analyses or the Kruskal-Wallis test by ranks, and post hoc comparisons were performed using the Mann-Whitney U test with a Bonferroni correction. Two-tailed $p < 0.05$ was considered to be significant.

ACCESSION NUMBERS

Transcriptional data are available under GEO accession number GSE66454.

SUPPLEMENTAL INFORMATION

Supplemental Information for this article includes Supplemental Experimental Procedures, four figures, and three movies and can be found with this article online at http://dx.doi.org/10.1016/j.stem.2015.03.004.

AUTHOR CONTRIBUTIONS

T. Takebe and H.Y.Y. conceived the study, designed the experiments, collected and analyzed the data, and wrote the manuscript. M.E., E.Y., and M.K. equally contributed to this work. M.E., E.Y., M.K., H.K., Y.U., T.M., T.Y., and T. Toyohara performed the experiments with the technical guidance and expertise of T. Takebe and H.Y.Y. K.O., H.N., and H.T. provided advice on the research strategy.

ACKNOWLEDGMENTS

We thank M. Kurimoto, N. Sasaki, Y. Takahashi, T.-S. Rashid, K. Sekine, Y.-W. Zheng, and the members of our laboratory for support. This work was mainly supported by PRESTO, Japan Science and Technology Agency (JST) (T. Takebe) and partly by Grants-in-Aid from the Ministry of Education, Culture, Sports, Science and Technology of Japan (nos. 24106510 and 24689052 to T. Takebe, nos. 24680050 and 24106505 to H.Y.Y., and nos. 21249071 and 25253079 to H.T.). This work was also partly supported by the JST through its research grant Research Center Network for Realization of Regenerative Medicine and a grant from the Japan IDDM network to K.O. and H.T. T. Takebe and H.T. have served on scientific advisory boards for Healios Inc. T. Takebe and H.T. have also granted a license to Healios through Yokohama City Univercity over their inventions that relate to the subject of this manuscript. T. Takebe and H.T. are conducting research under the collaborative research agreement with Healios and the subject of the research also relates to the subject of this manuscript. H.N. is a founder and shareholder of iCELL Inc. and ChimaERA Corp. and a founder, shareholder, and a scientific advisor for ReproCELL Inc.

Received: May 27, 2014
Revised: January 5, 2015
Accepted: March 13, 2015
Published: April 16, 2015

REFERENCES

Bertet, C., Sulak, L., and Lecuit, T. (2004). Myosin-dependent junction remodelling controls planar cell intercalation and axis elongation. Nature *429*, 667–671.

Besser, A., and Schwarz, U.S. (2007). Coupling biochemistry and mechanics in cell adhesion: a model for inhomogeneous stress fiber contraction. New J. Physiol. *9*, http://dx.doi.org/10.1088/1367-2630/9/11/425.

Conti, M.A., Even-Ram, S., Liu, C., Yamada, K.M., and Adelstein, R.S. (2004). Defects in cell adhesion and the visceral endoderm following ablation of nonmuscle myosin heavy chain II-A in mice. J. Biol. Chem. *279*, 41263–41266.

Ding, Q., and Cowan, C.A. (2013). Liver in a dish. Cell Res. *23*, 1242–1243.

Discher, D.E., Janmey, P., and Wang, Y.L. (2005). Tissue cells feel and respond to the stiffness of their substrate. Science *310*, 1139–1143.

Donà, E., Barry, J.D., Valentin, G., Quirin, C., Khmelinskii, A., Kunze, A., Durdu, S., Newton, L.R., Fernandez-Minan, A., Huber, W., et al. (2013). Directional tissue migration through a self-generated chemokine gradient. Nature *503*, 285–289.

Dourdin, N., Bhatt, A.K., Dutt, P., Greer, P.A., Arthur, J.S., Elce, J.S., and Huttenlocher, A. (2001). Reduced cell migration and disruption of the actin cytoskeleton in calpain-deficient embryonic fibroblasts. J. Biol. Chem. *276*, 48382–48388.

Eiraku, M., Takata, N., Ishibashi, H., Kawada, M., Sakakura, E., Okuda, S., Sekiguchi, K., Adachi, T., and Sasai, Y. (2011). Self-organizing optic-cup morphogenesis in three-dimensional culture. Nature *472*, 51–56.

Forgacs, G., Foty, R.A., Shafrir, Y., and Steinberg, M.S. (1998). Viscoelastic properties of living embryonic tissues: a quantitative study. Biophys. J. *74*, 2227–2234.

Fung, Y. (1993). Biomechanics: Material Properties of Living Tissues. (Springer).

Hackl, M.J., Burford, J.L., Villanueva, K., Lam, L., Suszták, K., Schermer, B., Benzing, T., and Peti-Peterdi, J. (2013). Tracking the fate of glomerular epithelial cells in vivo using serial multiphoton imaging in new mouse models with fluorescent lineage tags. Nat. Med. *19*, 1661–1666.

Lammert, E., Cleaver, O., and Melton, D. (2001). Induction of pancreatic differentiation by signals from blood vessels. Science *294*, 564–567.

Lancaster, M.A., and Knoblich, J.A. (2014). Organogenesis in a dish: modeling development and disease using organoid technologies. Science *345*, 1247125.

Liu, Z., Tan, J.L., Cohen, D.M., Yang, M.T., Sniadecki, N.J., Ruiz, S.A., Nelson, C.M., and Chen, C.S. (2010). Mechanical tugging force regulates the size of cell-cell junctions. Proc. Natl. Acad. Sci. USA *107*, 9944–9949.

Matsumoto, K., Yoshitomi, H., Rossant, J., and Zaret, K.S. (2001). Liver organogenesis promoted by endothelial cells prior to vascular function. Science *294*, 559–563.

Mizutani, T., Haga, H., Koyama, Y., Takahashi, M., and Kawabata, K. (2006). Diphosphorylation of the myosin regulatory light chain enhances the tension acting on stress fibers in fibroblasts. J. Cell. Physiol. *209*, 726–731.

Pouille, P.A., Ahmadi, P., Brunet, A.C., and Farge, E. (2009). Mechanical signals trigger Myosin II redistribution and mesoderm invagination in Drosophila embryos. Sci. Signal. *2*, ra16.

Raab, M., Swift, J., Dingal, P.C., Shah, P., Shin, J.W., and Discher, D.E. (2012). Crawling from soft to stiff matrix polarizes the cytoskeleton and phosphoregulates myosin-II heavy chain. J. Cell Biol. *199*, 669–683.

Sasai, Y. (2013a). Cytosystems dynamics in self-organization of tissue architecture. Nature *493*, 318–326.

Sasai, Y. (2013b). Next-generation regenerative medicine: organogenesis from stem cells in 3D culture. Cell Stem Cell *12*, 520–530.

Sato, T., and Clevers, H. (2013). Growing self-organizing mini-guts from a single intestinal stem cell: mechanism and applications. Science *340*, 1190–1194.

Schwab, K., Patterson, L.T., Aronow, B.J., Luckas, R., Liang, H.C., and Potter, S.S. (2003). A catalogue of gene expression in the developing kidney. Kidney Int. *64*, 1588–1604.

Shin, J.W., Buxboim, A., Spinler, K.R., Swift, J., Christian, D.A., Hunter, C.A., Léon, C., Gachet, C., Dingal, P.C., Ivanovska, I.L., et al. (2014). Contractile forces sustain and polarize hematopoiesis from stem and progenitor cells. Cell Stem Cell *14*, 81–93.

Shindo, A., and Wallingford, J.B. (2014). PCP and septins compartmentalize cortical actomyosin to direct collective cell movement. Science *343*, 649–652.

Shutova, M., Yang, C., Vasiliev, J.M., and Svitkina, T. (2012). Functions of nonmuscle myosin II in assembly of the cellular contractile system. PLoS ONE *7*, e40814.

Steinberg, M.S. (1962). On the Mechanism of Tissue Reconstruction by Dissociated Cells, Iii. Free Energy Relations and the Reorganization of Fused, Heteronomic Tissue Fragments. Proc. Natl. Acad. Sci. USA *48*, 1769–1776.

Straight, A.F., Cheung, A., Limouze, J., Chen, I., Westwood, N.J., Sellers, J.R., and Mitchison, T.J. (2003). Dissecting temporal and spatial control of cytokinesis with a myosin II Inhibitor. Science *299*, 1743–1747.

Suga, H., Kadoshima, T., Minaguchi, M., Ohgushi, M., Soen, M., Nakano, T., Takata, N., Wataya, T., Muguruma, K., Miyoshi, H., et al. (2011). Self-formation of functional adenohypophysis in three-dimensional culture. Nature *480*, 57–62.

Takebe, T., Sekine, K., Suzuki, Y., Enomura, M., Tanaka, S., Ueno, Y., Zheng, Y.W., and Taniguchi, H. (2012). Self-organization of human hepatic organoid by recapitulating organogenesis in vitro. Transplant. Proc. *44*, 1018–1020.

Takebe, T., Sekine, K., Enomura, M., Koike, H., Kimura, M., Ogaeri, T., Zhang, R.R., Ueno, Y., Zheng, Y.W., Koike, N., et al. (2013). Vascularized and functional human liver from an iPSC-derived organ bud transplant. Nature *499*, 481–484.

Takebe, T., Kobayashi, S., Suzuki, H., Mizuno, M., Chang, Y.M., Yoshizawa, E., Kimura, M., Hori, A., Asano, J., Maegawa, J., and Taniguchi, H. (2014a). Transient vascularization of transplanted human adult-derived progenitors promotes self-organizing cartilage. J. Clin. Invest. *124*, 4325–4334.

Takebe, T., Zhang, R.R., Koike, H., Kimura, M., Yoshizawa, E., Enomura, M., Koike, N., Sekine, K., and Taniguchi, H. (2014b). Generation of a vascularized and functional human liver from an iPSC-derived organ bud transplant. Nat. Protoc. *9*, 396–409.

Takeichi, M. (2011). Self-organization of animal tissues: cadherin-mediated processes. Dev. Cell *21*, 24–26.

Wolf, K., Mazo, I., Leung, H., Engelke, K., von Andrian, U.H., Deryugina, E.I., Strongin, A.Y., Bröcker, E.B., and Friedl, P. (2003). Compensation mechanism in tumor cell migration: mesenchymal-amoeboid transition after blocking of pericellular proteolysis. J. Cell Biol. *160*, 267–277.